Communication

Short-Chain Acid Additives to Control PbI$_2$ Crystallization in Hybrid Perovskite Films

Chiara Dionigi [1],* , Gabriele Calabrese [2] , Giampiero Ruani [1] and Silvia Milita [2]

1   Consiglio Nazionale delle Ricerche, Istituto per lo Studio dei Materiali Nanostrutturati (ISMN), Via P. Gobetti 101, I-40129 Bologna, Italy

2   Consiglio Nazionale delle Ricerche, Istituto per la Microelettronica e Microsistemi (IMM), Via P. Gobetti 101, I-40129 Bologna, Italy

*   Correspondence: chiara.dionigi@cnr.it

Abstract: The quality and the performance of hybrid perovskite (HP)'s films strongly depend on the complete conversion into MAPbI$_3$ of a spin-coated solution of methylammonium iodide (MAI) and PbI$_2$. Highly crystalline PbI$_2$ on a substrate limits such a conversion and, consequently, the HP's solar cell performances. We investigate for the first time the use of short-chain organic acids as additives in a non-complexing solvent like γ-butyrolactone (GBL), that can retard retard the crystallization of PbI$_2$. Based on XRD analyses of the spin coated films, the acetic acid is the most effective additive in retarding the PbI$_2$ crystallization, making Pb^{2+} available for a subsequent reaction with MAI. These results open a new experimental path for fabricating perovskite films by single or sequential step methods involving acid additives.

Keywords: perovskite; films; PbI$_2$ crystallization; solar cells; short chain acids

1. Introduction

The study of hybrid perovskite (HP) structure and applications is extensively dominating the current photovoltaic scene due to their exceptional properties [1–3] along with low production costs. However, HPs suffer from poor environmental and thermal stability, and very often from inadequate quality of the polycrystalline films in terms of traps and grain boundaries, which dramatically affect the performance of the photovoltaic devices [4,5].

A single step or a sequential two-step deposition method has been applied for the fabrication of films of lead perovskites.

The single step uses a mixture of PbX$_2$ and CH$_3$NH$_3$X in common solvents like dimethyl sulfoxide (DMSO), dimethylformamide (DMF), and γ-butyrolactone (GBL), as well as in combinations. The solvents used to prepare hybrid lead halide perovskites strongly influence the crystallization process of perovskite [6]. Indeed, the coordination and the binding ability of the solvents affect the formation of the intermediate adducts with the metal ion. Moreover, the solvent's boiling point controls the evaporation rate and drives the nucleation/crystallization mechanism that strongly influences the film structures and morphology [7].

However, obtaining thin films with suitable characteristics through low-cost solution processing is not trivial because the uncontrolled deposition of the HP reagents can occur, producing a significant variation in the morphology and the composition of the films reducing the prospects for practical applications [8]. In particular, PbI$_2$ can remain after the thermal treatment of the film as an unreacted residual or as a by-product of the CH$_3$NH$_3$PbI$_3$ (hereafter called MAPI), degradation [9], whereas the organic cation CH$_3$NH$_3$I (hereafter called MAI) volatilizes or decomposes at temperature above 110 °C [10].

In the two-step sequential deposition of MAPI, PbI$_2$ is first deposited on a substrate from a solution and subsequently transformed into the perovskite by exposing it to a solution of CH$_3$NH$_3$I [11]. The arrangement of PbI$_2$ on the substrate is essential for the

quality of the resulting HP films. When PbI_2 results in a uniform amorphous film it is ready to completely react with the organic component (CH_3NH_3I) to generate perovskite crystals at the second step within few minutes [11].

As reported in the literature, strong interactions between the solvent and Pb^{2+} and the high solubility of PbI_2 hamper the formation of crystalline PbI_2 in the solvent and consequentially in the film [11–14].

The PbI_2 crystals can be separated from the reagent solution for either the one-step or for the two-steps deposition.

For the first time in MAPI film fabrication, we investigated the use of complexing organic agents able to sequestrate Pb^{2+} from the solution retarding the crystallization of PbI_2.

Long-chain carboxylic acids have been previously reported as a colloidal synthesis strategy for lead halide nano-sheets with a thickness below 100 nm [15,16].

The tendency of the carboxylic group of each acid to interact with Pb^{2+} is strictly connected with the polarity of the carboxyl group, which strongly influences the resulting carboxylic acid constant (K_a, often reported as Cologarithm pK_a) [17,18].

A very important factor that determines even considerable variations in the polarity of carboxyl group and consequently in the pK_a, is the type of group bound to the carboxyl: the electron-attractors cause a decrease in pK_a while the groups electron donors increase it. Conversely, the alkyl groups ($-CH_3$) are weakly electron-repulsive and they accentuate the negative charge on the oxygen of the carboxylate ion, determining a decrease in acidity. For this reason, the acetic acid (CH_3COOH) is about one order of magnitude weaker than formic acid ($HCOOH$) and for the same reason also, the pK_a of the long-chain carboxylic acids that were adopted for the synthetic colloidal strategy falls within the same 4–5 range of pK_a [17].

The anchoring effect of carboxylic acids on perovskite has recently attracted significant attention in the production of more resistant hybrid perovskite for solar cells. In particular, the formic acid is active in controlling the colloidal size and free ion concentration in precursor solution towards the formation of large crystals in the functional films. Moreover, the addition of fluorinated carboxylic acids plays a crucial role in modulating the grain size, film quality, and crystallinity of perovskite films. Additionally, it improves the hydrophobicity of the perovskite layer and increases the ambient stability of the device by surface passivation [19–22].
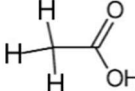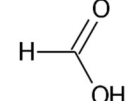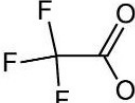
Although the length of the carboxylic acid chain is determinant in developing the colloidal suspension that determines the PbI_2 arrangement in nano-sheets and peculiar geometries [15,16], such as rings, the literature on the complexing effect of short-chain carboxylic acids is more limited [19–21].

With the aim of controlling the generation of amorphous PbI_2, we applied short-chain carboxylic acids as additives in the single-step deposition of HP on the ITO substrate. To select the best performing short-chain acid additive, we chose GBL as the solvent because of its poor coordination properties on the precursors that do not interfere with the improvement due to the coordination of the acid additive. Moreover, the low solubility of the precursors in GBL can highlight the complexing effect of the additive. We chose FORMIC ACID, ACETIC ACID and TRIFLUOROACETIC ACID, which are similar short-chain acids in structure and dimensions but with significantly different acidity.

2. Results and Discussion

The morphology of the starting series of thin films prepared as reported in Table 1, Materials & Methods section, was captured by scanning electron microscopy (Figure 1) at two different magnifications.

Table 1. Acid additives details.

| Acid Name	Structure	Film Name	Molar Mass (g/mol)	Boiling Temperature (°C)	Density (g/cm^3)	pKa *	Added Acid (μL)
NO-ACID		O	#	#	#	#	0
Acetic		A	60	118	1.05	4.74	7.5
Formic		B	46	100.8	1.22	3.75	4.7
Trifluoroacetic		C	114	72.4	1.49	−0.25	10.0

* Cologarithm of acid dissociation constant.
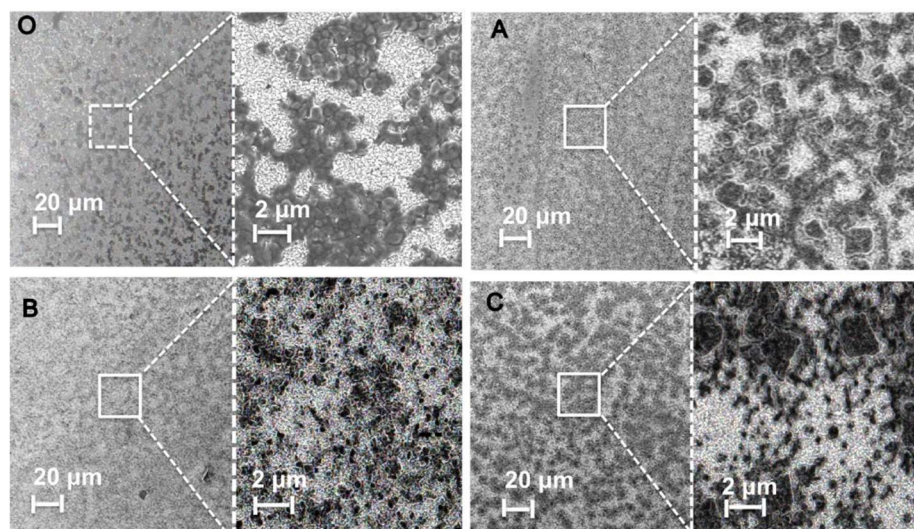
Figure 1. SEM images (top view) at different magnifications of films prepared under the conditions reported the Materials & Methods section. The films are named O (no acid additive), A (acetic acid), B (formic acid), C (trifluoracetic acid).

From the SEM images, it is evident that the films are not uniform but consist of round domains of sub-micrometer size, very often coalescing in larger islands. Despite the differences in the acid additives, all the starting films are very similar in appearance.

It is worthy noting that SEM images at maximum magnification do not show micrometresized PbI$_2$ sheets or rings having a uniform hexagonal shape from 2 μm to 10 μm, as reported in the case of PbI$_2$ colloidal suspensions from long-chain carboxylic acids [15,16].

On these films, specular XRD patterns were recorded in air immediately after the thermal treatment in controlled atmosphere (to limit the deterioration process). As reported in Figure 2, the XRD patterns of all the deposited films in GBL, named A, B, C, O with and without additives, show diffraction peaks corresponding to the 110, 211, 202, 220, 310, 224, and 314 reflections of an orthorhombic perovskite crystalline structure. The analysis of the relative intensity of the different reflections indicates that the majority of crystallites are randomly oriented, with only weak preferential orientation with the (110) parallel to the surface, as commonly observed in MAPI films [23]. Additionally, the presence of the peak corresponding to the 001 reflection of PbI$_2$ demonstrates that the conditions adopted for the film fabrication produce a mixture of MAPI and PbI$_2$.
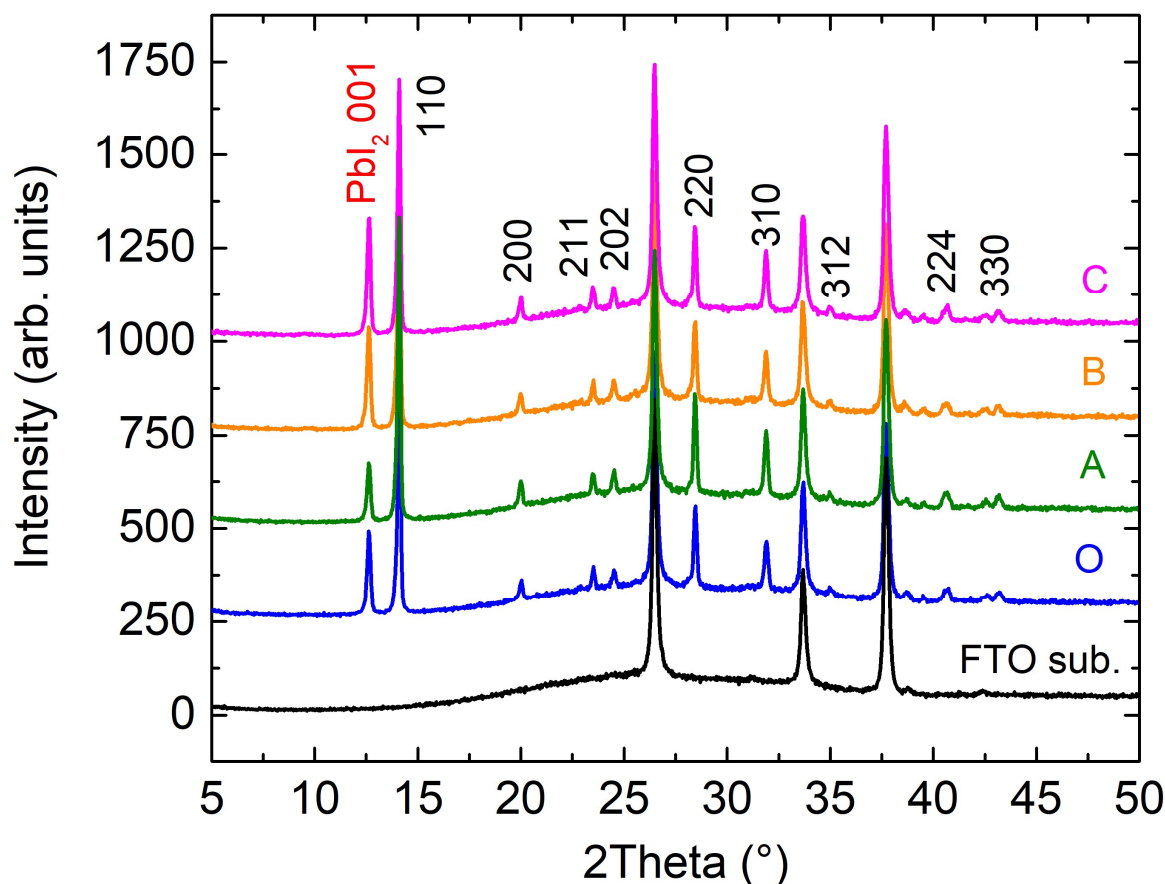
Figure 2. XRD patterns of the deposited films, in γ-butyrolactone with acid additives after the thermal treatment in nitrogen atmosphere (RH 20 ± 3%). The films are named O (no acid additive), A (acetic acid), B (formic acid) and C (trifluoracetic acid).

To evaluate if the acid addition could be an effective method of retarding the PbI_2 crystallization and leave PbI_2 available to react with the MAI in ambient conditions, we followed the approach reported by J. Burschka et al. [11]. We tested all the films by dipping them into a solution of MAI (10 mg ml^{-1}) in anhydrous 2-propanol for 20 s followed by rinsing in 2-propanol. Afterwards, the films were fast dried under nitrogen flux. All these treatments were performed in ambient conditions. After the treatment the films were named O_1, A_1, B_1 and C_1.

The XRD patterns recorded after the dipping treatment with MAI (Figure 3), show that the O_1, B_1, C_1 films maintained the PbI_2 phase, present only in traces in the film A_1. In the film O_1 the not complete MAPI formation is evidenced by the presence of MAI and $(CH_3NH_3)_4PbI_6 \bullet 2H_2O$ diffraction peaks, weakly visible also for C_1.

We tried a second attempt with film O_1, B_1, C_1 since the first attempt was not effective.

In the second treatment the time of immersion in MAI solution, was increased to 60 s. The films treated for the second time were renamed in O_2, B_2 and C_2.

As shown in Figure 4, strong peak corresponding to PbI_2 phase is visible for all the samples despite the additional treatment and the longer time of immersion.
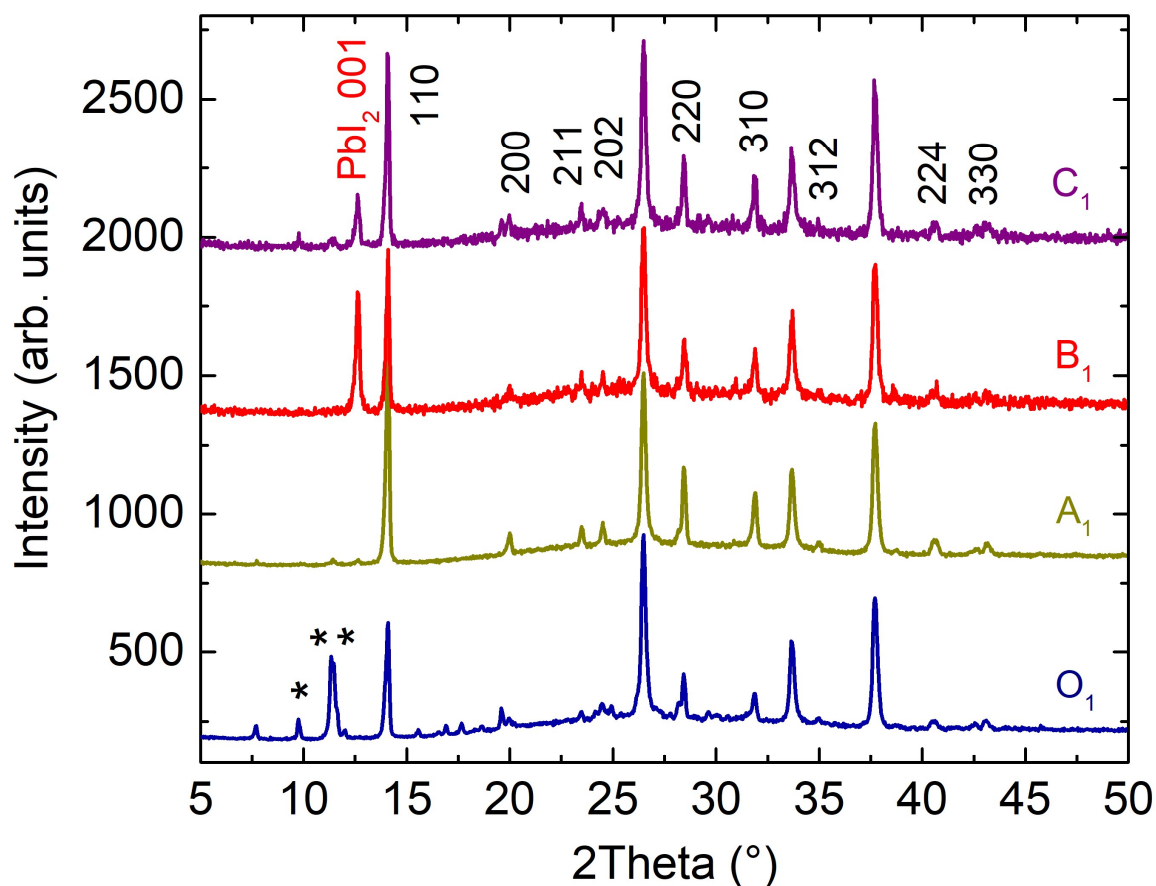
Figure 3. XRD patterns of films O (no acid additive), A (acetic acid), B (formic acid) and C (trifluoracetic acid), after the first dipping in MAI. The asterisks * and ** for film O_1 correspond to peaks 001 of MAI and $(CH_3NH_3)_4PbI_6 \bullet 2H_2O$, respectively, weakly visible for C_1.

The vertical dimension of the coherently diffracting domains was estimated by the analysis of the 110 peak, by using the Scherrer's equation and assuming Gaussian diffraction lines and a shape factor of 0.9. We obtain a vertical dimension of 47 nm for sample O, which slightly decreases, more or less, depending on the specific treatment to 37 nm (O_1 and O_2), 36 nm (A_1), 43 nm (B_1 and B_2) or 45 and 43 nm (C_1 and C_2). These results highlight that the exposition time to anhydrous 2-propanol, in the investigated time range, does not affect the crystalline size.

The relative amount of crystalline PbI_2 is determined by considering the ratio of the integrated area of the peak 100 of PbI_2 and that of the peak 110 of MAPI. For such analysis, Gaussian distribution functions are used to fit the diffraction peaks. The results of the analysis are reported in Table 2.

For film A (acetic acid as additive), this ratio attains the lowest value, indicating a lower content of crystalline PbI_2, and it even falls below the detection threshold after the treatment with MAI.

Since the same stoichiometry was used for all films, this points out to a reduced crystallization of PbI_2 in favor of the formation of amorphous PbI_2.
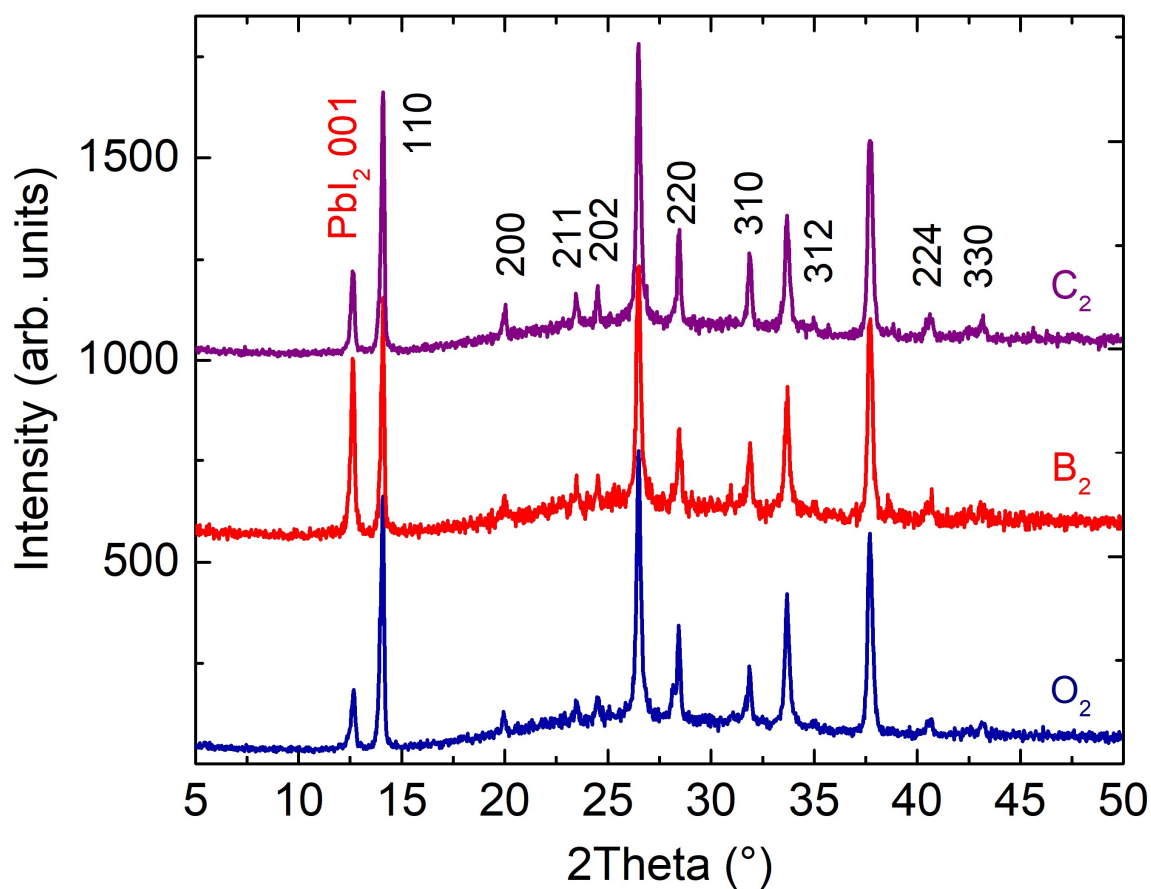
Figure 4. XRD patterns of films after the second dipping treatment in MAI.

Table 2. Integrated areas of 100 of PbI_2 and of 110 of MAPI and their ratio.

Film	PbI_2 100 Area (arb. Units)	MAPI 110 Area (arb. Units)	PbI_2 100/MAPI 110 (%)
O	42	112	38
A	29	135	21
B	53	118	45
C	59	112	53
O_1	-	90	0
A_1	-	157	0
B_1	87	100	87
C_1	34	122	28
O_2	31	128	24
B_2	90	101	89
C_2	42	120	35

On the other hand, with the MAI treatment, the content of crystalline PbI_2 in film C (trifluoroacetic acid as additive) decreases but never reduces to zero, and in film B (formic acid as additive), it even increases.

For the film prepared without additive the ratio decreases after the first treatment with MAI solution in ambient conditions, because no PbI_2 is observed but MAI and $(CH_3NH_3)_4PbI_6 \bullet 2H_2O$ are observed nevertheless a subsequent treatment induces PbI_2 crystallization.

On the bases of the literature on the control of PbI_2 crystallization [11,12], we can conclude that in the conditions adopted in the experiments, only the acetic acid is effective in retarding the PbI_2 crystallization.

The acetic acid and the trifluoroacetic acid have the same chain length (as reported in Table 1). On the other hand, the formic acid chain has only a slightly higher pK_a than the acetic acid as indicated by the different pk_a values: -1.25 of the TRIFLUOROACETIC ACID (the strongest), 3.75 of the FORMIC ACID (intermediate acidity) and 4.74 ACETIC ACID (lower acidity).

Although higher acidity corresponds to a higher polarity of the carboxylate groups, the pK_a does not seem to be the only factor in retarding the crystallization of PbI_2, since the most effective additive shows the highest pK_a among the selected additives.

Conversely, acetic acid is the only one, among the selected acidis, with a boiling point above the temperature, 110 °C, the temperature adopted for the thermal treatment of the films. The other two acid additives have a boiling point below 110 °C. The values reported for pure acids are not expected to increase significantly in an organic solvent according to the ebullioscopic constants and the boiling point elevation theory.

Hence, the permanence in the solution of the carboxylic acid deserves to be taken into account. In particular the evaporation of the acid additive upon thermal treatment at 110 °C of the spin-coated films has to be considered.

By fundamental chemical considerations, we can assert that in the same experimental conditions, the acid-additive with the boiling temperature above the treatment temperature (110 °C), remains longer in the liquid phase than the others. Hence, Pb^{2+} can stay longer sequestered by the carboxylate, which retards its crystallization.

Comparative investigations are underway to define an optimized procedure with acids of various boiling temperatures acids to implement the single and double-step MAPI deposition.

In conclusion, we propose a new approach to MAPI film fabrication based on controlling the reactivity of PbI_2 in the wet deposition through common acid additives.

We found that due to the physical characteristics, like its boiling temperature, acetic acid as an additive can efficiently sequestrate the cation (Pb^{2+}) from the reagent solution at a temperature below its boiling point and release it as reactive PbI_2 to the MAI. We believe this method that is based only on the physical characteristics of the acid additives could represent a novelty in solar cell fabrication.

3. Materials & Methods

3.1. Perovskite Film Preparation

Perovskite precursor solution was obtained by dissolving lead iodide (PbI_2) and methylammonium iodide (MAI) in γ-butyrolactone (GBL) at a concentration of 1 mol/L in a 1:1 molar ratio. The reagents were kept under stirring at 60 °C overnight to dissolve the salts. The solution was filtered using a nylon filter with 0.45-μm pore size to obtain transparent solution hereafter called MAPI.

3.2. Adding Selected Acids

Following the literature, where acids were considered in the bulk crystallization, we decided to add 5.3×10^{-4} moles of the selected acid per 1×10^{-3} moles of the reagents in the equimolar GBL solution [24].

Each acid was added to 0.5 mL of the MAPI solution immediately before the deposition by spin coating on ITO substrate. The chemical characteristics of the selected acids, together with structures, and the amount of each acid added to 0.5 mL of MAPI, are reported in Table 1.

3.3. Film Deposition

The deposition was performed in a glove box in a nitrogen atmosphere by spin coating 25 μL of each solution on 1×1 cm Fluorine doped tin oxide coated glass slide (FTO) as

substrates. Afterwards they were placed in the middle of a preheated hot plate at 110 °C for 70 min. The relative humidity in the glove box was $20 \pm 3\%$ during the entire process.

3.4. Film Characterization

Scanning electron microscopy (SEM) characterization.

SEM observations on as prepared samples were performed using a Zeiss FEG-SEM LEO 1530 electron microscope at 5 kV equipped with an Oxford INCA energy dispersive X-ray spectrometer for elemental analysis.

XRD measurements.

Film structure was characterized by performing specular XRD θ/2θ measurements by using a SmartLab-Rigaku diffractometer, equipped with a rotating anode (CuKα_1, λ = 1.54180 Å) followed by a parabolic mirror, to collimate the incident beam, and a series of variable slits (placed before and after the sample position) resulting in an angular divergence of the diffracted beam of 0.03°. A 0D point detector is used to collect the diffracted beam.

References

1. Mathews, N.; Sun, S.; Lim, S.S.; Lam, Y.M.; Gräetzel, M.; Mhaisalkar, S.; Sum, T.C. Long-Range Balanced Electron- and Hole-Transport Lengths G. Xing in Organic-Inorganic CH NH PbI. *Science* **2013**, *342*, 344.
2. Lee, M.M.; Teuscher, J.; Miyasaka, T.; Murakami, T.N.; Snaith, H.J. Efficient Hybrid Solar Cells Based on Meso-Superstructured Organometal Halide Perovskites. *Science* **2012**, *338*, 643–647. [CrossRef]
3. Chen, C.; Li, C.; Li, F.; Wu, F.; Tan, F.; Zhai, Y.; Zhang, W. Efficient perovskite solar cells based on low temperature solution-processed (CH3NH3)PbI3perovskite/CuInS2 planar heterojunctions. *Nanoscale Res. Lett.* **2014**, *9*, 457. [CrossRef] [PubMed]
4. Fan, Z.; Xiao, H.; Wang, Y.; Zhao, Z.; Lin, Z.; Cheng, H.-C.; Lee, S.-J.; Wang, G.; Feng, Z.; Goddard, W.A.; et al. Layer-by-Layer Degradation of Methylammonium Lead Tri-iodide Perovskite Microplates. *Joule* **2017**, *1*, 548–562. [CrossRef]
5. Azpiroz, J.M.; Mosconi, E.; Bisquert, J.; De Angelis, F. Defect Migration in Methylammonium Lead Iodide and Its Role in Perovskite Solar Cell Operation. *Energy Environ. Sci.* **2015**, *8*, 2118–2127. [CrossRef]
6. Huang, P.-H.; Wang, Y.-H.; Ke, J.-C.; Huang, C.-J. The Effect of Solvents on the Performance of $CH_3NH_3PbI_3$ Perovskite Solar Cells. *Energies* **2017**, *10*, 599. [CrossRef]
7. Fateev, S.A.; Petrov, A.A.; Khrustalev, V.N.; Dorovatovskii, P.V.; Zubavichus, Y.V.; Goodilin, E.A.; Tarasov, A.B. Solution Processing of Methylammonium Lead Iodide Perovskite from γ-Butyrolactone: Crystallization Mediated by Solvation Equilibrium. *Chem. Mater.* **2018**, *30*, 5237–5244. [CrossRef]
8. Im, J.-H.; Lee, C.-R.; Lee, J.-W.; Park, S.-W.; Park, N.-G. 6.5% efficient perovskite quantum-dot-sensitized solar cell. *Nanoscale* **2011**, *3*, 4088–4093. [CrossRef]
9. Niu, G.; Guo, X.; Wang, L. Review of recent progress in chemical stability of perovskite solar cells. *J. Mater. Chem. A* **2015**, *3*, 8970. [CrossRef]
10. Wang, K.; Ecker, B.; Huang, J.; Gao, Y. Evaporation of Methylammonium Iodide in Thermal Deposition of MAPbI$_3$. *Nanomaterials* **2021**, *11*, 2532. [CrossRef]
11. Burschka, J.; Pellet, N.; Moon, S.-J.; Humphry-Baker, R.; Gao, P.; Nazeeruddin, M.K.; Grätzel, M. Sequential deposition as a route to high-performance perovskite-sensitized solar cells. *Nature* **2013**, *499*, 316. [CrossRef] [PubMed]
12. Wu, Y.; Islam, A.; Yang, X.; Qin, C.; Liu, J.; Zhang, K.; Peng, W.; Han, L. Retarding the crystallization of PbI$_2$for highly reproducible planar-structured perovskite solar cells via sequential deposition. *Energy Environ. Sci.* **2014**, *7*, 2934–2938. [CrossRef]
13. Jeon, N.J.; Noh, J.H.; Kim, Y.C.; Yang, W.S.; Ryu, S.; Seok, S.I. Solvent engineering for high-performance inorganic–organic hybrid perovskite solar cells. *Nat. Mater.* **2014**, *13*, 897–903. [CrossRef] [PubMed]

14. Chen, Q.; Zhou, H.; Hong, Z.; Luo, S.; Duan, H.-S.; Wang, H.-H.; Liu, Y.; Li, G.; Yang, Y. Planar Heterojunction Perovskite Solar Cells via Vapor-Assisted Solution Process. *J. Am. Chem. Soc.* **2014**, *136*, 622–625. [CrossRef] [PubMed]

15. Klein, E.; Heymann, L.; Hungria, A.B.; Lesyuka, R.; Klinke, C. Colloidal lead iodide nanorings. *Nanoscale* **2018**, *10*, 21197–21208. [CrossRef]

16. Klein, E.; Lesyuk, R.; Klinke, C. Insights into the formation mechanism of two-dimensional lead halide nanostructures. *Nanoscale* **2018**, *10*, 4442. [CrossRef]

17. Hsiao, C.-P.; Siebert, K.J. Modelling the inhibitory effects of organic acids on bacteria. *Int. J. Food Microbiol.* **1999**, *47*, 189–201. [CrossRef]

18. Bala, T.; Prasad, B.L.V.; Sastry, M.; Kahaly, M.U.; Waghmare, U.V. Interaction of Different Metal Ions with Carboxylic Acid Group: A Quantitative Study. *J. Phys. Chem. A* **2007**, *111*, 6183–6190. [CrossRef]

19. Gupta, R.K.; Garai, R.; Iyer, P.K. Ambient St Perovskite Solar Cells through Trifluoro Acetic Acid-Mediated Multifunctional Anchoring. *ACS Appl. Energy Mater.* **2022**, *5*, 1571–1579. [CrossRef]

20. Zhu, H.; Duan, C.; Qin, M.; Liu, Z.; Li, J.; Yuan, L.; Wen, Q.; Lu, X.; Shi, L.; Xie, J.; et al. Trifluoromethylphenylacetic Acid as In Situ Accelerant of Ostwald Ripening for Stable and Efficient Perovskite Solar Cells. *Sol. RRL* **2021**, *5*, 2100040. [CrossRef]

21. Meng, L.; Wei, Q.; Yang, Z.; Yang, D.; Feng, J.; Ren, X.; Liu, Y.; Liu, S. (Frank). Improved perovskite solar cell efficiency by tuning the colloidal size and free ion concentration in precursor solution using formic acid additive. *J. Energy Chem.* **2020**, *41*, 43–51. [CrossRef]

22. Adil Afroz, M.; Ghimire, N.; Reza, K.M.; Bahrami, B.; Bobba, R.S.; Gurung, A.; Chowdhury, A.H.; Iyer, P.K.; Qiao, Q. Thermal Stability and Performance Enhancement of Perovskite Solar Cells Through Oxalic Acid-Induced Perovskite Formation. *ACS Appl. Energy Mater.* **2020**, *3*, 2432–2439. [CrossRef]

23. Foley, B.J.; Girard, J.; Sorenson, B.A.; Chen, A.Z.; Niezgoda, J.S.; Alpert, M.R.; Harper, A.F.; Smilgies, D.-M.; Clancy, P.; Saidie, W.A.; et al. Controlling nucleation, growth, and orientation of metal halide perovskite thin films with rationally selected additives. *J. Mater. Chem. A* **2017**, *5*, 113. [CrossRef]

24. Nayak, P.K.; Moore, D.T.; Wenger, B.; Nayak, S.; Haghighirad, A.A.; Fineberg, A.; Noel, N.K.; Reid, O.G.; Rumbles, G.; Kukura, P.; et al. Mechanism for rapid growth of organic–inorganic halide perovskite crystals. *Nat. Commun.* **2016**, *7*, 13303. [CrossRef] [PubMed]